Dynamics of Water Confined Within Reverse Micelles

Daniel E. Rosenfeld and Charles A. Schmuttenmaer*

Yale University, Department of Chemistry, 225 Prospect St., P.O. Box 208107, New Haven, Connecticut 06520-8107

Received: January 25, 2006; In Final Form: May 22, 2006

We report structural and dynamical properties of water confined within reverse micelles (RMs) ranging in size from $R = 10$ Å to $R = 23$ Å as determined from molecular dynamics simulations. The low-frequency infrared spectra have been calculated using linear response theory and depend linearly on the fraction of bulklike water within the RMs. Furthermore, these spectra show nearly isosbestic behavior in the region near 660 cm^{-1}. Both of these characteristics are present in previously measured experimental spectra. The single dipole spectra for interfacial trapped, bound, and bulklike water within the RMs have also been calculated and show region-dependent frequency shifts. Specifically, the bound and trapped water spectra have a peak at lower frequencies than that for the inner core water. We therefore assign the low-frequency band in the IR spectra to bound and trapped interfacial water. Finally, region-dependent hydrogen bonding profiles and spatial distribution functions are also presented.

1. Introduction

It is well-known that liquids confined to nanometer-scale dimensions or smaller behave differently than their bulk counterparts. Water is no exception. Understanding the origin of these differences is essential due to the importance of water trapped in clays, zeolites, porous glasses, and even within proteins. Reverse micelles (RMs) provide an ideal system for probing the effects of confinement on the properties of water. In a RM, a confined water pool is created within an organic solvent. Surfactant molecules with an ionic or polar headgroup and hydrophobic tail mediate the water−solvent interaction and prevent bulk phase separation.

The most commonly studied RM is water/NaAOT/*iso*-octane. It is comprised of a nanoscopic water pool, surrounded by sodium aerosol OT [sodium bis(2-ethylhexyl) sulfosuccinate] surfactant, and dispersed in *iso*-octane solvent. Thus, this is the system we have chosen to model. The diameter of the water pool can be experimentally varied from about 0.3 nm to about 12 nm by adjusting w_0, the water to surfactant molar ratio: w_0 = water/surfactant. It has been shown that the RM size varies nearly linearly with w_0.[1]

This type of RM has been studied by many experimental methods, including FTIR,[2−5] NMR,[6,7] fluorescence spectroscopy,[8] quasi-elastic neutron scattering,[9] light scattering,[1,10] and ultrafast infrared vibrational echo spectroscopy.[11,12] Various properties have been measured as a function of size, such as the OH stretching band of water,[2,13,14] the librational band of water,[3] relaxation dynamics of dye molecules trapped within the water pool,[8,15−17] and the far-infrared spectrum.[18,19] The majority of these studies suggest systems comprised of two or three water states. In the two-state systems, the water is either bound or bulklike, and in the three-state systems, the water is trapped, bound, or bulklike.

When using ionic surfactants, the role of the counterions must also be considered. For example, the effective Na^+ concentration is almost 14 molar in a RM with $w_0 = 4$. In comparison, a saturated aqueous sodium chloride solution is roughly 6 molar. Clearly, there exists the possibility that the behavior of the water is affected by the high ionic concentration in addition to any confinement effects. It is found that the counterions are largely confined to the interface due to the attraction from the negatively charged headgroups. Thus, the ionic concentration toward the center of the RM is quite moderate. Furthermore, the positive and negative charges of the counterions and headgroups largely cancel each other out, so that only the water in interfacial region is significantly affected.

Venables et al. previously showed that the librational infrared absorbance band of water trapped within a series of RM sizes exhibits an isosbestic point, suggesting a two-state system in equilibrium (see Figure 1).[3] This two-state behavior was verified by a global linear least-squares fitting procedure which showed that the spectra as a function of RM size were linear combinations of the bound water and free, or bulklike, water spectra. In bulk water, the librational band is at about 680 cm^{-1}, and the bound water exhibited an absorbance peak that was red-shifted from the bulk peak by about 200 cm-^{1}.[3]

In addition to experimental studies, several computational studies have been carried out to obtain information not directly measurable experimentally.[9,20−28] For example, Tobias and Klein simulated RMs formed from water, calcium carbonate, and a metal sulfonate surfactant. These micelles were simulated in CCl_4, octane, and vacuum and were shown to be essentially spherical.[28]

Faeder and Ladanyi have performed numerous simulations using a simplified model for water and AOT RMs in *iso*-octane.[22−25] The micelles simulated have ranged from $w_0 = 1$ to $w_0 = 10$. Their model assumes that a spherical cavity is filled with water, counterions, and surrounded by surfactant headgroups, which are radially constrained to define the interface.[23] They have used this model to calculate structural and some basic dynamical properties of the RMs. The water within the simulated micelles exhibits a radial stratification into trapped, bound, and bulklike regions. The trapped water molecules are confined to

* To whom correspondence should be addressed. E-mail: charles.schmuttenmaer@yale.edu.

10.1021/jp060552p CCC: $33.50
Published on Web 07/01/2006

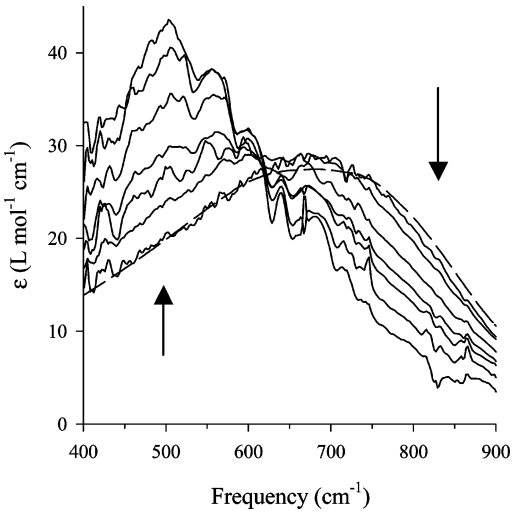

Figure 1. Experimentally measured molar extinction coefficient spectra of water confined within RMs of various sizes. The progression of sizes from large to small is indicated with the arrows. Bulk water is shown with the smooth curve, followed by RMs with $w_0 = 40$, 20, 10, 6, 4, 2, and 1. Reprinted with permission from ref 3. Copyright 2001 American Chemical Society.

the interfacial region and are coordinated, on average, to a single headgroup.[23] The bound layer is strongly perturbed by the highly charged interface, and the bulklike water pool is insulated from the interface by the bound layer. There is facile interchange between these latter two regions. There is an increase in water−water hydrogen bonding as the distance from the interface increases. These structural calculations have been performed with both sodium and potassium counterions, and interfacial trapping of water has been shown to depend on counterion radius.[22]

The solvation response has also been calculated for iodine-like chromophores,[25] and results have shown that the interface exerts strong electrostatic forces on charged sites within the micelle interior. The time scale of the solvation response is also strongly dependent on w_0, wherein larger RMs have faster (more bulklike) responses. This is attributed to the increased mobility and bulklike character of the water pools within larger RMs.[24,25] Harpham et al. have calculated self-intermediate scattering functions for quasi-elastic neutron scattering (QENS) experiments which supports the validity of the assumptions by Faeder and Ladanyi.[9] The scattering functions were also calculated as a function of counterion type, demonstrating some dynamical dependence on counterion identity.[26] Faeder and Ladanyi, however, have not calculated many dynamical quantities, such as the infrared spectrum, for water confined within RMs, nor fully investigated the regionally dependent rotational dynamics of the confined water.

Senapati and Berkowitz have simulated water in a RM created by a fluorosurfactant with a phosphate headgroup and supercritical carbon dioxide as the solvent.[27] They have shown that there is a perturbation to the water−water hydrogen bonding network at the interface, and that the interfacial water forms hydrogen bonds with the oxygen atoms of the headgroup. The sluggish rotational and translational dynamics of interfacial water are also discussed. They characterize the rotational dynamics through the exponential decay of the average single-molecule dipole moment autocorrelation function.

The dynamical properties of confined water depend strongly on RM size as well, yet have not received the same level of attention as structural properties. We report the calculated librational absorption spectrum for RMs with w_0 ranging from 1 to 10. The librational spectrum is chosen because it can be calculated using *rigid* molecules. Also, the simulated results can be directly compared with experimentally measured librational spectra.[3] In addition to the calculated absorption spectra, we present the single dipole spectra for water molecules in different regions of the RM. We deconstruct the region-specific dynamics of water confined within RMs as manifested in librational absorbance, single-dipole spectra, spatial distribution functions, and hydrogen bonding.

TABLE 1: Sizes and Numbers of Molecules for the Various Simulations Performed.[a]

	n_{water}	$n_{Z,Na}$	R (Å)
$w_0 = 1$	21	21	10.25
$w_0 = 2$	52	26	11.40
$w_0 = 3$	96	32	13.25
$w_0 = 4$	140	35	14.10
$w_0 = 7.5$	525	70	19.40
$w_0 = 10$	980	98	22.90
HC_{140}	140	0	10.01

[a] HC_{140} represents 140 water molecules in a hydrophobic cavity with a 10.01 Å radius and includes only the influence of the wall potential.

TABLE 2: Interaction Potential Parameters. the Lennard-Jones Radius and Well Depth Are Given by σ and ϵ, Respectively, and q is the Charge on a Particular Site

	σ (Å)	ϵ/k_B (K)	q (e)
O	3.166	78.24	−0.8476
H			0.4238
Na^+	2.275	58.01	1.0
Z^-	6.0	251.58	−1.0
wall	2.5	231.55	

2. Computational Methods

2.1. Model Details. Molecular dynamics simulations of water/NaAOT/*iso*-octane RMs have been performed using the model introduced by Faeder and Ladanyi.[23] RMs have been simulated ranging in radius from 10.25 to 22.9 Å with w_0 values ranging from 1 to 10, respectively (see Table 1 for details).

The model consists of SPC/E water,[29] sodium counterions, and unified atom headgroups representing the SO_3^- ions. The *z*-axis is the symmetry axis of the water molecule, the *y*-axis is its out-of-plane axis, and the *x*-axis is its in-plane axis. The headgroups are constrained to the surface of the RM by a harmonic potential. All parameters are given in Table 2. A continuum wall potential is also included to simulate the interaction of the interior with the exterior *iso*-octane continuum. The intersite potential is a standard Lennard−Jones potential plus an electrostatic term,

$$U_{ij}(r) = 4\epsilon_{ij}\left[\left(\frac{\sigma_{ij}}{r_{ij}}\right)^{12} - \left(\frac{\sigma_{ij}}{r_{ij}}\right)^{6}\right] + \frac{q_i q_j}{r_{ij}} \quad (1)$$

where ϵ_{ij} and σ_{ij} are defined by the standard Lorentz−Berthelot combining rules,

$$\epsilon_{ij} = \sqrt{\epsilon_i \epsilon_j},\ \sigma_{ij} = \frac{\sigma_i + \sigma_j}{2} \quad (2)$$

The harmonic potential is specified by the relation,

$$U(r) = \frac{1}{2}k(R - r - d_e)^2 \quad (3)$$

where r is the radial distance, k is 600 kcal mol^{-1}, and d_e is 2.5 Å. The minimum of this harmonic potential defines the interface.

The wall potential was calculated by Faeder and Ladanyi in the same manner as Linse and Halle by integrating a continuum of Lennard−Jones sites over a spherical cavity.[23,30] The exact form of the potential is given by,

$$U(z) = 18\sqrt{3}\epsilon_{\text{wall}}\left[\frac{15}{2}\left(\frac{\sigma_{\text{wall}}}{R}\right)^9 F(z,6) - \left(\frac{\sigma_{\text{wall}}}{R}\right)^3 F(z,3)\right] \quad (4)$$

where $F(z,6)$ and $F(z,3)$ are given by,

$$F(z,3) = 2[3(1 - z^2)^3]^{-1}$$

$$F(z,6) = 2(5 + 45z^2 + 63z^4 + 15z^6)[45(1 - z^2)^9]^{-1} \quad (5)$$

where $z = r/R$.[23] The wall potential was calculated using the same σ_{wall} and ϵ_{wall} for both sodium and oxygen sites within the micelle. Following Faeder and Ladanyi, the values of σ_{wall} and ϵ_{wall} have been taken from Lee et al.[31] Wall interaction potential parameters are also summarized in Table 2.

2.2. Simulation Details. The equations of motion were integrated using the leapfrog version of the Verlet algorithm. This includes the leapfrog integration method using quaternions for the rigid body motion of the water molecules.[32] The system was coupled to a Berendsen thermostat with a 1.0 ps time constant during the equilibration periods and a 2.0 ps time constant during the accumulation of data.[33] A 2.0 fs time step was used throughout the simulations. Data were accumulated during 2.0 ns of simulation trajectories after equilibration.

The RMs were constructed by a method similar to the one used by Faeder and Ladanyi.[23] The number of particles in the RM and the radius were obtained from interpolation of light scattering data measured by Eicke and Rehak and the use of average molecular volumes for H_2O (30 Å^3), Z^- (57 Å^3), and Na^+ (6 Å^3).[10,23] First, the headgroups were evenly distributed on a sphere of appropriate radius using an approximative algorithm.[34] The sodium counterions were then randomly placed throughout the RM, and simulated annealing was performed from 1000 K down to 0 K. At the end of the annealing, a distribution of headgroups and counterions were present at the interface. Randomly oriented water was then placed within the micelle on a cubic lattice inscribed within the sphere formed by the headgroups. The system was then equilibrated at 500 K for 600 ps, followed by a linear decrease in temperature over 400 ps to 298.2 K, at which point the system was equilibrated for an additional 600 ps. The temperature of the system during data acquisition at times beyond 1.2 ns was 298.2 K. As Faeder and Ladanyi previously note, we find that, although there is some dependence for specific micelle observables (ensemble average energies, ionic layer structures) on construction parameters, the structural and dynamical characteristics are invariant as long as the system has reached equilibrium.[23]

Bulk water was also simulated using 216 SPC/E water molecules at 298.2 K at a concentration of 55.39 mol/L using the MolDy program written by Keith Refson with a Nose−Hoover thermostat.[35] Programs developed by the authors were used for RM simulations.

2.3. The Frequency-Dependent Dielectric Permittivity. The primary goal of this paper is to make comparisons of the calculated IR spectra of water trapped within RMs with experimental data. This comparison is accomplished through the linear response treatment for the frequency-dependent dielectric for classical dipolar systems with mobile ions developed by Caillol et al.[36] Their treatment predicts the dielectric to depend primarily upon the total dipole moment autocorrelation function and the total ionic current autocorrelation function. By incorporating the total ionic current correlation function, Caillol et al. account for the response of charge carriers to the electric field within the system. Since the RMs are highly ionic we prefer this treatment over other methods of calculating absorbance. We refer the interested reader to the Supporting Information available online for further discussion of other methods. Caillol et al. treat both periodic boundary conditions and spherical systems. This paper utilizes the result for systems of spherical geometry for the calculations involving RMs and the periodic boundary conditions result for the calculation involving bulk water.

In particular, the spherical geometry considered by Caillol and co-workers is a spherical volume suspended in a continuous dielectric medium. For our calculations, we use *iso*-octane as our continuous dielectric. Since *iso*-octane interacts weakly with low-frequency electric fields, the complex frequency-dependent dielectric function is approximated by the static dielectric constant of 1.936.[37] Following Caillol, the complex dielectric function for spherical systems is given by

$$\eta(\omega) = \epsilon(\omega) + \frac{4\pi i\sigma(\omega)}{\omega} \quad (6)$$

where $\eta(\omega)$ is the frequency-dependent *generalized* permittivity, $\epsilon(\omega)$ is the frequency-dependent permittivity, and $\sigma(\omega)$ is the frequency-dependent conductivity. Note, each of these three quantities is complex-valued. The following relationships are used to calculate $\epsilon(\omega)$ and $\sigma(\omega)$:

$$\left[\frac{2\Sigma^*(\omega) + 3}{2\Sigma^*(\omega) + 3 + \Sigma(\omega)}\right]\frac{\epsilon(\omega) - 1}{4\pi} = \frac{\beta}{3V}[\langle \mathbf{M}_W^2\rangle + i\omega\int_0^\infty \langle \mathbf{M}_W(t)\cdot\mathbf{M}_W(0)\rangle e^{i\omega t}dt + \int_0^\infty \langle \mathbf{M}_W(t)\cdot\mathbf{J}_I(0)\rangle e^{i\omega t}dt] \quad (7)$$

$$\left[\frac{2\Sigma^*(\omega) + 3}{2\Sigma^*(\omega) + 3 + \Sigma(\omega)}\right]\sigma(\omega) = \frac{\beta}{3V}[\int_0^\infty \langle \mathbf{J}_I(t)\cdot\mathbf{J}_I(0)\rangle e^{i\omega t}dt + i\omega\int_0^\infty \langle \mathbf{J}_I(t)\cdot\mathbf{M}_W(0)\rangle e^{i\omega t}dt] \quad (8)$$

where $\Sigma(\omega) = \eta(\omega) - 1$ and

$$\mathbf{M}_W(t) = \sum_i \mathbf{m}_i(t) \quad (9)$$

$$\mathbf{J}_I(t) = \sum_j q_j\mathbf{v}_j(t) \quad (10)$$

where i and j are sums over the dipolar molecules and ions respectively, and the asterisk (*) denotes the properties of the dielectric continuum. We note that the functions Σ^* and Σ are the electric susceptibilities of the solvent and the system respectively within a factor of 4π**;** these factors arise in the solution of the field equations for the system, and we refer the reader to ref 34 for additional details. For a periodic simulation, the relations remain the same, except that the fractions containing Σ^* and Σ in front of $\epsilon(\omega)$ and $\sigma(\omega)$ in eqs 7 and 8 are equal to 1. The complex refractive index, $\hat{n}(\omega) = n(\omega) - ik(\omega)$, is the square root of the generalized complex dielectric permittivity [$\eta(\omega)$ in eq 6]. The frequency-dependent absorption coefficient is obtained from the imaginary part of the complex index of refraction, $k(\omega)$, using $\alpha(\omega) = 2\omega k(\omega)/c$, where c is the speed of light in a vacuum. The absorbance spectra have been scaled by the concentration of the water in the RM to yield the molar

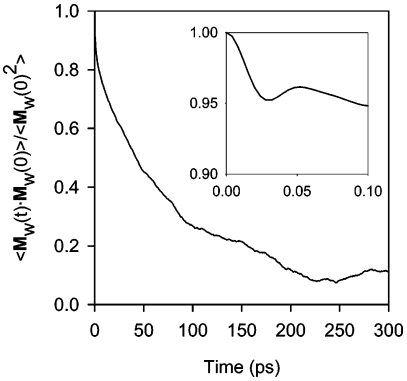

Figure 2. The total water dipole moment time autocorrelation function from $t = 0$ to $t = 300$ ps for the $w_0 = 7.5$ micelle. The function decays slowly and requires windowing to eliminate truncation error. The inset is the same function from $t = 0$ to $t = 0.1$ ps which illustrates the time domain oscillation that corresponds to the librational motion of the water molecules.

absorption coefficient, ϵ, of the water molecules (not to be confused with the permittivity).

We note that for a periodic simulation of bulk water where there are no mobile ions, the complex permittivity is given by the relation,

$$\frac{\epsilon(\omega) - 1}{4\pi} = \frac{\beta}{3V}[\langle \mathbf{M}_W{}^2 \rangle + i\omega \int_0^\infty \langle \mathbf{M}_W(t) \cdot \mathbf{M}_W(0) \rangle e^{i\omega t} dt] \quad (11)$$

Equation 11 can also be used with single-molecule dipole autocorrelation functions to determine approximate infrared absorbance spectra for water. For example, it has been used previously to characterize regional dynamics in supercooled water,[38] and the spectrum of water in binary mixtures.[39]

One complication in this calculation is the long nonexponential decay of the micellar total water dipole moment autocorrelation function, as shown in Figure 2. Because the time scale of the librational motion is roughly 0.1 ps, the autocorrelation function was calculated for 300 ps, all of which was windowed using the Welch windowing function.[40] This windowing function decreases to zero quadratically and eliminates truncation error. The nonexponential decay also occurs for single-molecule dipole functions which were also windowed. The Laplace transforms were carried out numerically using standard methods of quadrature. All dielectric calculations were performed in the electrostatic cgs unit system.

2.4. Single Dipole Infrared Spectra. One limitation in the calculation of the total system infrared absorbance spectrum is that spectral contributions by species in different regions of the RM cannot be resolved, which is precisely the same limitation encountered in the experimental spectra. However the dynamics of a region of the system can be probed by analyzing the single dipole moment autocorrelation function for molecules within the region, even though region-dependent spectra cannot be measured experimentally.

The single dipole autocorrelation functions, $\langle \mathbf{m}_i(t) \cdot \mathbf{m}_i(0) \rangle$, were computed for each of the three RM regions: trapped, bound, and bulklike. These regions were identified based on criteria developed previously by Faeder and Ladanyi.[23] Trapped water is found within 1.5 Å of the interface ($d \leq 1.5$ Å), bound water is found between 1.5 Å $< d < m_3$, where m_3 is the third minimum in the radial density distribution, and bulklike water is found at $d \geq m_3$, where d is the distance from the interface. The correlation functions were calculated only when a molecule was found in a particular region continuously from time 0 to time t. This differs from the method used by Faeder and Ladanyi for their calculations of the single-molecule dipole moment ACF which suffered from the problem of particle exchange between regions. Since particles can exchange from the bulklike to the bound water pools on the time scale of librational relaxation, our method includes only those fluctuations which represent true bulklike or bound behavior. The absorbance was calculated from the permittivity obtained from eq 11. Correlation functions of 25 ps in length were used for the single-dipole spectra calculations in the different RM regions.

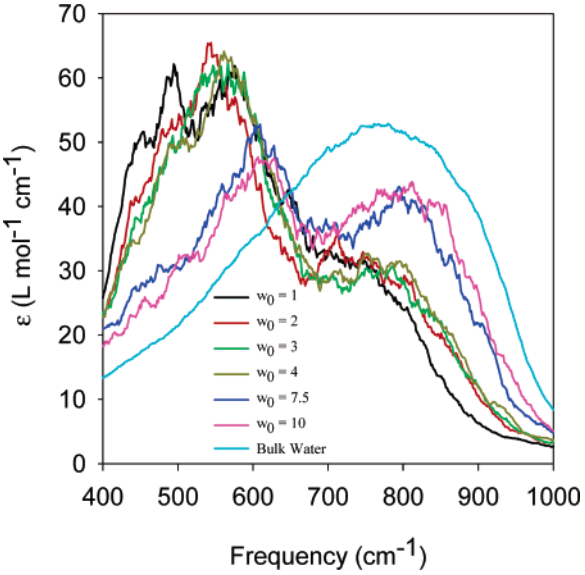

Figure 3. The calculated molar absorbance spectrum of the librational band for water confined to micelles of different sizes and for bulk water.

3 Results and Discussion

3.1. The Infrared Absorbance Spectrum. The infrared absorbance spectra of RMs ranging from $w_0 = 1$ to $w_0 = 10$ as well as bulk water were calculated, and are plotted in Figure 3. These spectra have been smoothed using a 21 point moving average. The spectra show nearly isosbestic behavior, although the unresolved isosbestic region between 600 and 700 cm^{-1} is not quite as pronounced as in the experimental spectra. The spectra also show clear growth in the high-frequency band of the absorbance spectra as RM size increases. The librational spectra have very little dependence on the ionic motions, as shown in Figure 4. For example, when the ionic current time correlation functions are set to zero, lower frequency features below 400 cm^{-1} associated with the ionic conductivity disappear, but the librational spectra do not change significantly. The role of ionic conductivity will be the subject of a future publication.

The intensities of the calculated librational spectra are greater than their experimental counterparts. For example, the experimental bulk water molar extinction coefficient is about 30 L mol^{-1} cm^{-1} at its peak near 680 cm^{-1}, while the calculated value is roughly 50 L mol^{-1} cm^{-1}. This discrepancy is primarily because the model uses a value of 1 for n^2, where n is the high-frequency limit of the index of refraction. Calculating the bulk water dielectric spectrum using the actual value of $n^2 = 1.79$, results in a peak extinction coefficient of roughly 37 L mol^{-1} cm^{-1}. However, when performing the calculations we have used $n^2 = 1$ for all spectra because the high-frequency index is unknown for RM systems. By performing all calculations identically, relative changes are still meaningful, even if the absolute spectrum is not identical to that measured experimentally.

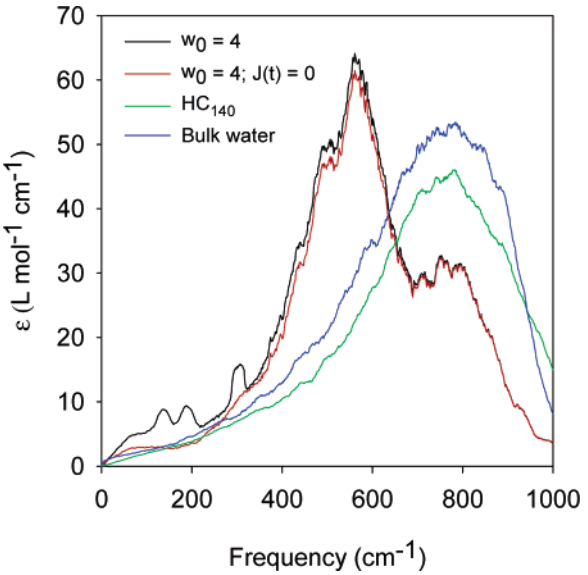

Figure 4. The calculated molar absorbance spectrum for $w_0 = 4$ RM, for $w_0 = 4$ RM when fixing the ionic current to zero, for HC_{140}, and for bulk water.

Experimentally, the librational infrared absorbance spectra show a linear dependence on the fraction of bulklike water, f_{bulk}, within the RM as determined by a global linear least-squares fit.[3] The quality of the fit resulted in the assignment of the spectra to a two-state system. In this simulation we have directly calculated f_{bulk} using the radial density profile of water within the RMs. If the simulated spectra are manifestations of a two-state system where one state is bulklike water and the other is a combination of trapped and bound water, then a global linear least-squares fit of the simulated spectra should result in values of f_{bulk} that agree with those obtained directly from the radial density profiles. Such a fit was performed by fixing $f_{bulk} = 1$ for the calculated bulk spectrum, and varying the fraction f_{bulk} for each RM spectrum as described previously.[3] Table 3 reports $f_{bulk,s}$ calculated directly from the radial density profiles, and $f_{bulk,r}$ determined by linear regressions of the simulated spectra. These values are in good agreement which validates the assumptions made in the simulations since the simulated and experimental absorbance spectra show the same trends, shifts, and linear dependence on f_{bulk}.

As indicated in Table 1, a spherical hydrophobic cavity of 10.01 Å radius consisting of 140 water molecules was also simulated. The only external force on the water molecules was the hydrophobic wall potential. The calculated infrared spectrum for the hydrophobic cavity shown in Figure 4 has a slight decrease in intensity and no red-shift relative to bulk water. This is consistent with the only slightly decreased hydrogen bonding near a hydrophobic interface.[23]

3.2. Single Dipole Spectra. The single dipole time autocorrelation functions have also been calculated for each region (trapped, bound, and bulklike) within the RMs. The regional absorbance spectra have been calculated using eq 11. This method is an approximation that neglects the cross terms in the collective dipole moment correlation function but still provides insight into the internal dynamics of the RMs. However, any regionally dependent calculated spectrum will suffer from one approximation or another.

Figure 5 presents the single dipole spectra for $w_0 = 4$. These spectra are representative of the single dipole spectra of other sizes, and clearly illustrate the region-dependent dynamics. Water molecules which are closer to the interface present

TABLE 3: Fractional Populations of Water ($f_{trapped}$, f_{bound}, $f_{bulk,s}$) in the RMs[a]

	$f_{trapped}$	f_{bound}	$f_{bulk,s}$	$f_{bulk,r}$
$w_0 = 1$	0.279	0.633	0.089	0.051
$w_0 = 2$	0.310	0.500	0.192	0.139
$w_0 = 3$	0.336	0.407	0.257	0.154
$w_0 = 4$	0.336	0.381	0.283	0.198
$w_0 = 7.5$	0.222	0.300	0.477	0.584
$w_0 = 10$	0.189	0.266	0.545	0.672

[a] Calculated from the radial density, and the fraction of bulk-like water determined by a global linear least squares fit of the simulated absorbance data, $f_{bulk,r}$.

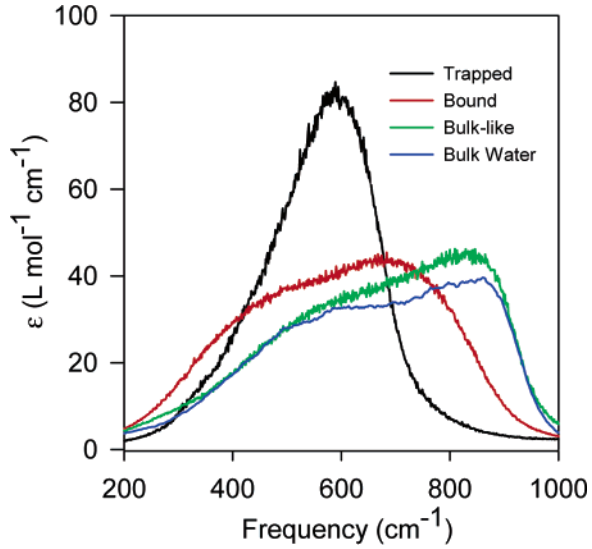

Figure 5. The calculated single-dipole spectra for regional water in $w_0 = 4$. The trapped, bound, bulklike, and bulk water spectra are black, red, green, and blue, respectively. There is a significant red-shift as the water approaches the interface.

significantly red-shifted librational frequencies. Figure 6 presents the single dipole spectra for each region (trapped, bound, and bulklike) across all micelle sizes ($w_0 = 1$ to $w_0 = 10$). In all cases the trapped and bound water spectra are red-shifted significantly from the spectrum of the bulklike region. Figure 6 reveals the general consistency of the librational dynamics of water within each region across micelle sizes. The spectra also demonstrate that the bulklike spectra approach the bulk water single dipole spectrum. The blue-shifting of the bound and trapped spectra as a function of RM size is consistent with the a slight increase in hydrogen bonding for these species that occurs for larger micelle sizes. We also note that the $w_0 = 1$ trapped water has a double peaked single dipole spectrum which we associate with the very large degree of perturbation at the interface in this micelle.

3.3. Hydrogen Bonding. Faeder and Ladanyi have previously calculated the radial dependence of hydrogen bonding in RMs with respect to w_0, and found a regional dependence of nearest neighbor interactions in AOT RMs.[23] We present similar calculations of the regional hydrogen bonding environments to reinforce the structural implications of our dynamical calculations. Hydrogen bonding information was obtained using standard geometrical criteria and sampling the configuration every 100 fs.[41] A hydrogen bond between a donating O−H group and an accepting oxygen (Z) was counted if $r_{Z-H} < 2.6$ Å, $r_{Z-O} < 3.5$ Å, and the H−O—Z angle was less than 30°. For an accepting headgroup (Z) the values were $r_{Z-H} < 4.0$ Å, $r_{Z-O} < 5.0$ Å with the same required angle.

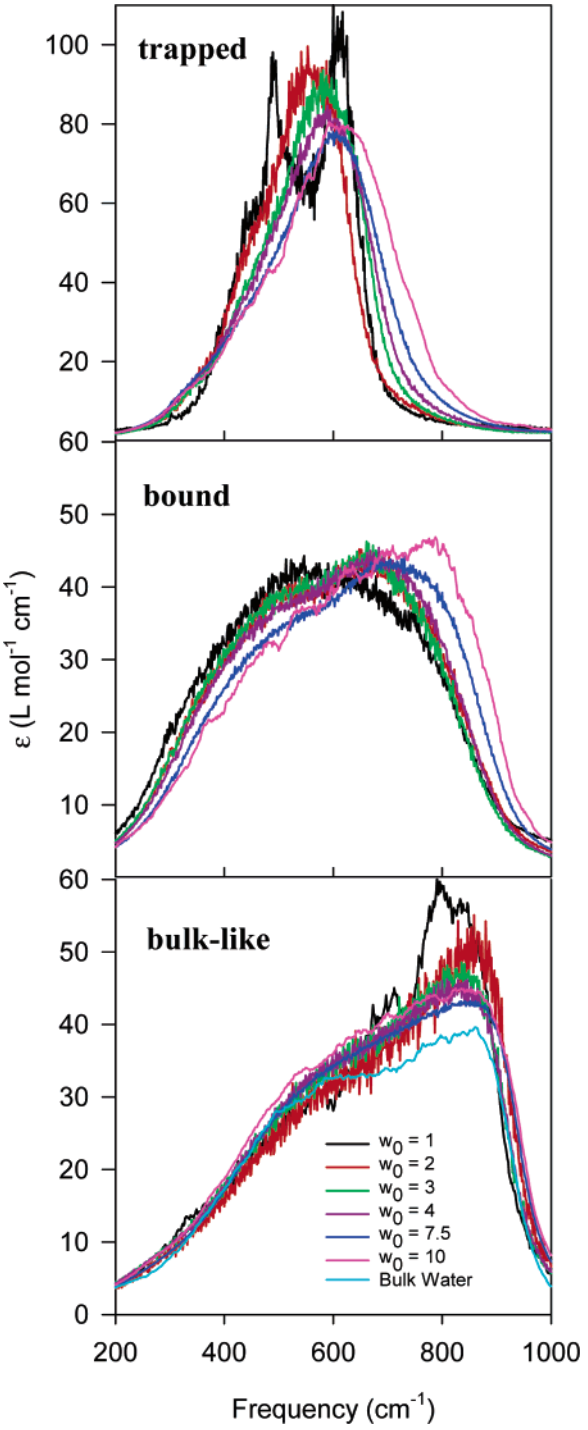

Figure 6. Single dipole spectra for $w_0 = 1$ through $w_0 = 10$ for trapped, bound, and bulklike regions. The spectra illustrate that regional librational dynamics are essentially conserved across micelle sizes. Other trends include the broadening and slight blue-shift of the bound and trapped peaks at larger RM sizes which is consistent with increased hydrogen bonding. Also, in the $w_0 = 1$ micelle the trapped water shows two peaks, which indicates the high degree of perturbation due to the local trapped environment.

The region-dependent water−water hydrogen bonding data are presented in Figure 7. The bulklike water has the most hydrogen bonding, the trapped water has the least, and the bound water is between that of bulklike and trapped. The bulklike water in the $w_0 = 1$ RM has the least hydrogen bonding of any of the RM bulklike water, but still has more hydrogen bonding than the $w_0 = 1$ bound water. These trends are preserved across RM sizes suggesting the conservation of hydrogen bonding motifs

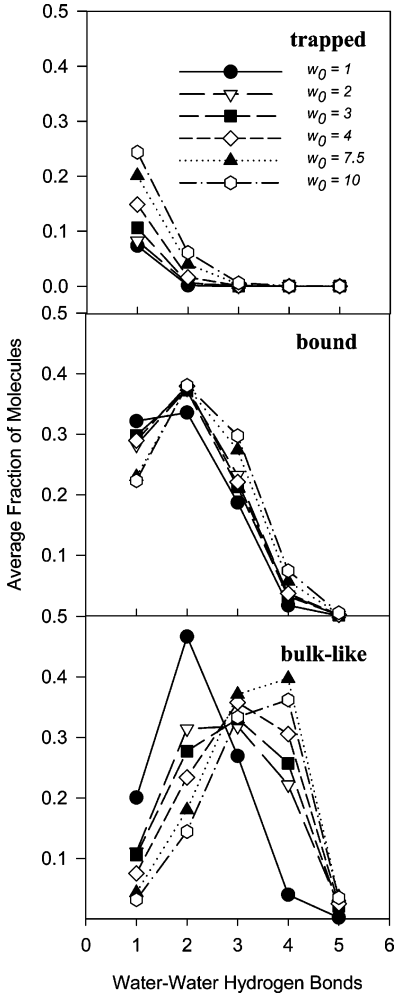

Figure 7. Average population of water−water hydrogen bonding states for trapped, bound, and bulklike water for various values of w_0. The regional hydrogen bonding environments are generally conserved across micelle sizes with the minor exception of bulklike water in $w_0 = 1$. There is a general increase in hydrogen bonding as the RM size increases which corresponds to an increase in molar concentration and progression toward bulklike properties.

across different values of w_0. As Faeder and Ladanyi previously note, water inside a micelle is generally of slightly lower density than bulk water so the hydrogen bonding is correspondingly lower.[23]

These results agree with the single dipole spectra as they confirm the correlation between hydrogen bonding environment and the characteristic frequencies of motion. Regions with less hydrogen bonding have correspondingly lower frequencies of angular motion. This result is also consistent with the experimental data previously measured.[3] The experimental spectra predict less hydrogen bonding in perturbed (bound and trapped) water, which this model has replicated.

3.4. Spatial Distribution of Local Environments. Since hydrogen bonding and the librational frequency are correlated, it is useful to visualize the local environment of water to provide further insight into structural aspects that correlate with librational properties. This visualization is performed through the calculation of spatial distribution functions for each of the radial regions. The 3-D plots themselves were made using GOpenMol.[42−44]

Figure 8 depicts the average structure of trapped water in the simulated RMs. The spatial distribution functions (SDFs) illustrate the large influence of Coulombic forces exerted by

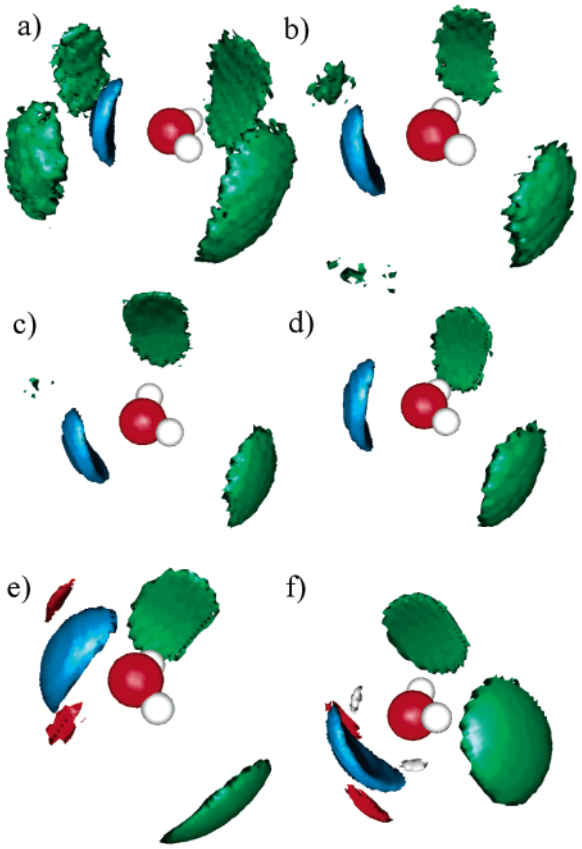

Figure 8. The structure of trapped water in a RM. The images are SDFs of trapped water for RMs with $w_0 = 1, 2, 3, 4, 7.5, 10$ in a−f, respectively. The green surfaces represent headgroups; the blue surfaces represent sodium counterions; the red surfaces represent oxygen; the white surfaces represent hydrogen. There is no appreciable density of hydrogen. The contours represent isodensity surfaces of 0.05Å^{-3} for the headgroups and 0.1Å^{-3} for sodium and oxygen. 50% of the molecules are only donating one hydrogen bond to a headgroup at a time, but the hydrogen sites are equivalent so the average density is distributed evenly. The appearance of oxygen density in $w_0 = 7.5$ is attributed to the increasing mobility of the trapped layer as RM size increases.

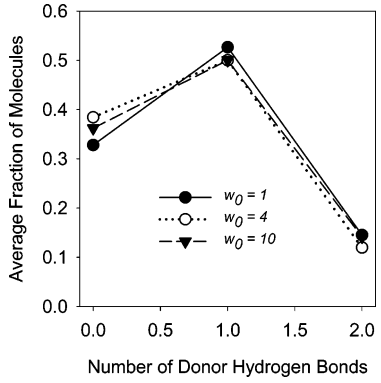

Figure 9. Average number of molecules populating a particular hydrogen bond donation state to headgroups for trapped water in $w_0 = 1, 4, 10$. These distributions are representative of the other micelles as well. Most of the molecules donate a single hydrogen bond.

the headgroups and counterions in the interfacial region. The lack of water−water hydrogen bonding in the trapped region (Figure 7) is evident in the SDFs where essentially all interactions are with headgroups and counterions. Figure 9 illustrates that the calculated probability of a trapped water donating a hydrogen bond to a single headgroup is five times higher than that for donation to two headgroups, but since both hydrogens

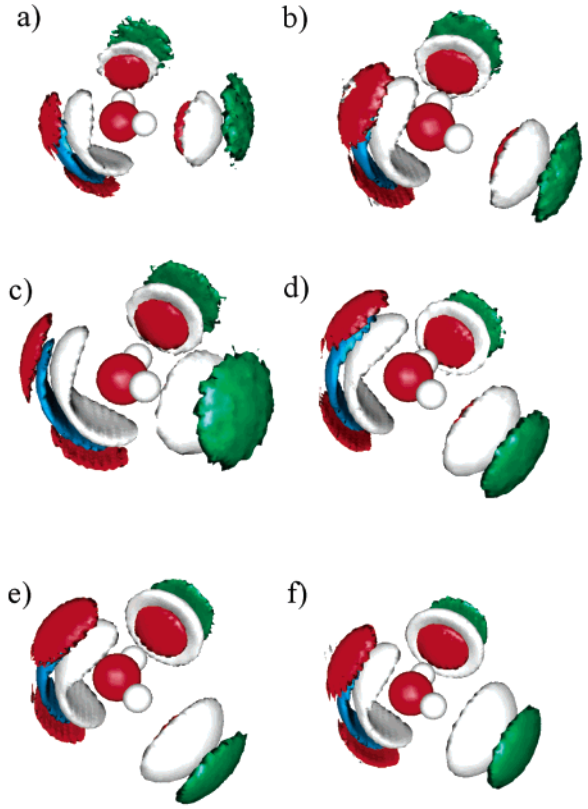

Figure 10. The structure of bound water in a RM. The contours represent isodensity surfaces of 0.1Å^{-3} for oxygen, sodium, and hydrogen. The headgroup contours are 0.025 Å^{-3} isodensity surfaces. The bound water shows a preference for perpendicular orientation of the O−H bond axis with respect to the interfacial layer. The bound layer also has strong interactions with the sodium counterions.

are equivalent, the spatial distribution density in Figure 8 is evenly distributed along both O−H bonds. The prevalence of single hydrogen bond donation was noted by Faeder and Ladanyi.[23]

Figure 10 shows SDFs for the bound water layer within the RMs. There is a nonzero density of headgroups receiving hydrogen bonds from the bound water molecules. The headgroup density indicates a propensity for the water to orient itself with its O−H bond vector normal to the surface for some time. The anisotropic density in the molecular frame indicates that the perturbation from the interface strongly affects the bound water layer. Faeder and Ladanyi also find a degree of orientation of the bound water. They also calculate the polarization density projected along the surface normal vector as a function of interfacial distance and demonstrate that both the trapped and bound layer are highly oriented in the RM.[23]

Figure 11 displays the SDFs for bulklike water within the RMs. The bulklike water pool is distant from the interface and does not interact strongly with it. One might expect the long range Coulombic interactions to affect the average orientation of the water. However, it is found that the headgroup density is negligible with respect to the isodensity surfaces plotted, and is essentially spherical. The bulklike water is electrostatically shielded from the headgroups by the intervening counterions and water.

The local environment of the three regions display regional trends which correlate with the hydrogen bond data and single dipole spectra presented above. The trapped region is essentially excluded from any bulklike hydrogen bonding network due to both solvation of the counterions and interaction with the

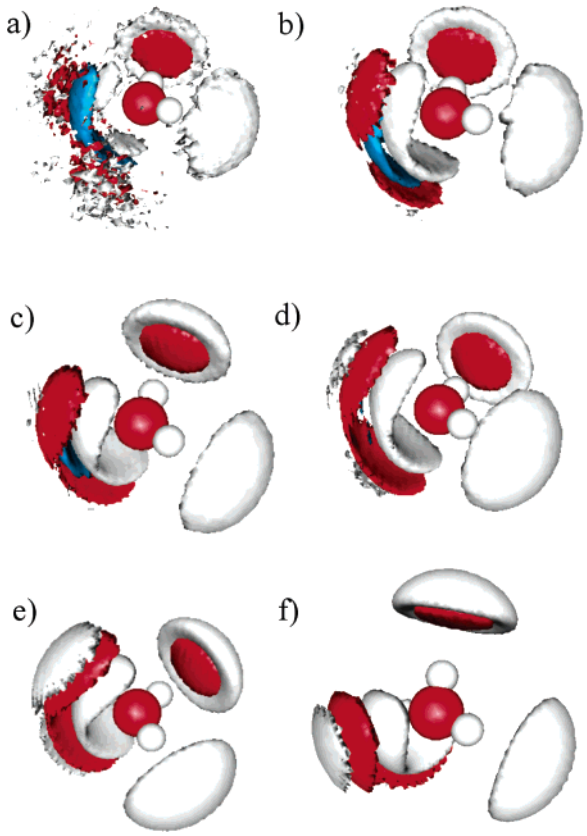

Figure 11. The structure of bulklike water in a RM. The contours represent isodensity surfaces of 0.1 $Å^{-3}$ for oxygen, sodium, and hydrogen. There is negligible headgroup density around the bulklike water molecules, indicating the lack of headgroup interaction with water in the core of the RM. In the smaller RMs there is significant ionic penetration into the bulklike water pool indicated by the sodium density.

surfactant headgroups, and shows the largest spectral red-shift. The bound region is highly perturbed by the interface and has a headgroup-dependent orientation. In the bound region, the headgroups also partially exclude other waters from accepting hydrogen bonds. These perturbations relative to free or bulklike water are manifested in a significant red-shift of the single dipole spectra. The bulklike water pool is not strongly perturbed by the interface. It has a spatial distribution similar to bulk water solvating a low concentration of ions, and a single dipole spectrum similar to that of bulk water.

4. Conclusions

We have carried out molecular dynamics simulations of water/AOT reverse micelles from $w_0 = 1$ to $w_0 = 10$ and have calculated their librational infrared absorbance spectra. These size-dependent spectra are in good agreement with experimental measurements.[3] The spectra show near-isosbestic behavior between an absorbance band at low frequency (500 cm^{-1}) and one at high frequency (800 cm^{-1}). The intensities of these two bands depend linearly on the fraction of bulklike water contained within the RMs. The agreement between the calculated and measured spectra has allowed detailed analysis of the simulation results.

First, the single-dipole spectra of water in different regions of the simulated RMs shift to lower frequency with closer proximity to the water/surfactant interface. The shift in frequency is essentially independent of w_0, and depends only on whether the water is in the trapped, bound, or bulklike region. These results illustrate the important role of the ionic interface on the dynamical behavior of water in the three different regions. Even though the net sodium ion concentrations are higher in the RMs considered here than even a supersaturated bulk solution, the spectra are not affected in the way expected for a homogeneous solution. This is because the majority of the ions are trapped at the interface by the negatively charged headgroups. Second, the trends in hydrogen bonding fractions and SDFs demonstrate decreasing water−water hydrogen bonding near the interface, with a concomitant increase in the interface-dependent orientation of water. Close to the interface, the bulk "structure" is highly perturbed by solvated ions, headgroups, and electrostatic interactions. These interactions fall off with increasing distance from the interface, and these perturbations are manifested dynamically in the single-dipole spectra, making a connection between structure and dynamics.

This study can be generalized to other confined and interfacial systems. The influence of the interface is far more important in confined systems than in bulk ones, since a confined system has a much larger fraction of molecules at or near the interface than does a bulk interface. A confined environment will strongly influence the librational dynamics of water, or more generally any hydrogen bonding liquid, *only* when there is significant perturbation of the liquid at the interface. Here, the perturbation is due to the ionic headgroups as well as the associated counterions defining the interface. This is illustrated in the interface-induced anisotropy of the bound and trapped water layers, the decrease in their water−water hydrogen bonding, and their red-shifted single-dipole spectra (none of these effects occur in the hydrophobic cavity). However, beyond a distance of about 4 Å from the interface, the behavior of water is essentially bulklike.

This paper has demonstrated the applicability of the water/AOT reverse micelle model presented by Faeder and Ladanyi[23] to dynamical calculations, and has demonstrated the accuracy of infrared absorbance calculations of ionic, nonperiodic systems such as RMs. In the future, it will be interesting to apply this method of calculating the frequency-dependent dielectric permittivity to similar RM systems. One example would be to investigate surfactants with dipolar rather than ionic headgroups. Another avenue entails investigating the influence of different counterions on the librational spectrum of water, paying special attention to region-specific dependencies. It would also be worthwhile to simulate the librational band of methanol containing RMs, as the size-dependent librational infrared spectra have already been measured.[3] Future work will also include a more detailed model in which the headgroups are treated atomistically. This will allow trapped water to bind to specific oxygen sites on the headgroup, and will better represent the interface.

Acknowledgment. We acknowledge the National Science Foundation (CHE-0135884) for partial support of this work. D.E.R. thanks the Arnold and Mabel Beckman Foundation for support under the Beckman Scholars Program.

Supporting Information Available: Calculation of infrared spectra from molecular dynamics simulations and the role of quantum corrections. This material is available free of charge via the Internet at http://pubs.acs.org.

References and Notes

(1) Zulauf, M.; Eicke, H. F. *J. Phys. Chem.* **1979**, *83*, 480.
(2) Onori, G.; Santucci, A. *J. Phys. Chem.* **1993**, *97*, 5430.
(3) Venables, D. S.; Huang, K.; Schmuttenmaer, C. A. *J. Phys. Chem. B* **2001**, *105*, 9132.

(4) Jain, T. K.; Varshney, M.; Maitra, A. *J. Phys. Chem.* **1989**, *93*, 7409.
(5) Temsamani, M. B.; Maeck, M.; El Hassani, I.; Hurwitz, H. D. *J. Phys. Chem. B* **1998**, *102*, 3335.
(6) Maitra, A. *J. Phys. Chem.* **1984**, *88*, 5122.
(7) Hauser, H.; Haering, G.; Pande, A.; Luisi, P. L. *J. Phys. Chem.* **1989**, *93*, 7869.
(8) Willard, D. M.; Riter, R. E.; Levinger, N. E. *J. Am. Chem. Soc.* **1998**, *120*, 4151.
(9) Harpham, M. R.; Ladanyi, B. M.; Levinger, N. E.; Herwig, K. W. *J. Chem. Phys.* **2004**, *121*, 7855.
(10) Eicke, H. F.; Rehak, J. *Helv. Chim. Acta* **1976**, *59*, 2883.
(11) Tan, H. S.; Piletic, I. R.; Fayer, M. D. *J. Chem. Phys.* **2005**, *122*.
(12) Tan, H. S.; Piletic, I. R.; Riter, R. E.; Levinger, N. E.; Fayer, M. D. *Phys. Rev. Lett.* **2005**, *94*.
(13) D'Angelo, M.; Onori, G.; Santucci, A. *J. Phys. Chem.* **1994**, *98*, 3189.
(14) Fioretto, D.; Freda, M.; Mannaioli, S.; Onori, G.; Santucci, A. *J. Phys. Chem. B* **1999**, *103*, 2631.
(15) Shirota, H.; Horie, K. *J. Phys. Chem. B* **1999**, *103*, 1437.
(16) Riter, R. E.; Willard, D. M.; Levinger, N. E. *J. Phys. Chem. B* **1998**, *102*, 2705.
(17) Willard, D. M.; Levinger, N. E. *J. Phys. Chem. B* **2000**, *104*, 11075.
(18) Boyd, J. E.; Briskman, A.; Sayes, C. M.; Mittleman, D.; Colvin, V. *J. Phys. Chem. B* **2002**, *106*, 6346.
(19) Mittleman, D. M.; Nuss, M. C.; Colvin, V. L. *Chem. Phys. Lett.* **1997**, *275*, 332.
(20) Abel, S.; Sterpone, F.; Bandyopadhyay, S.; Marchi, M. *J. Phys. Chem. B* **2004**, *108*, 19458.
(21) Brown, D.; Clarke, J. H. R. *J. Phys. Chem.* **1988**, *92*, 2881.
(22) Faeder, J.; Albert, M. V.; Ladanyi, B. M. *Langmuir* **2003**, *19*, 2514.
(23) Faeder, J.; Ladanyi, B. M. *J. Phys. Chem. B* **2000**, *104*, 1033.
(24) Faeder, J.; Ladanyi, B. M. *J. Phys. Chem. B* **2001**, *105*, 11148.
(25) Faeder, J.; Ladanyi, B. M. *J. Phys. Chem. B* **2005**, *109*, 6732.
(26) Harpham, M. R.; Ladanyi, B. M.; Levinger, N. E. *J. Phys. Chem. B* **2005**, *109*, 16891.
(27) Senapati, S.; Berkowitz, M. L. *J. Chem. Phys.* **2003**, *118*, 1937.
(28) Tobias, D. J.; Klein, M. L. *J. Phys. Chem.* **1996**, *100*, 6637.
(29) Berendsen, H. J. C.; Grigera, J. R.; Straatsma, T. P. *J. Phys. Chem.* **1987**, *91*, 6269.
(30) Linse, P.; Halle, B. *Mol. Phys.* **1989**, *67*, 537.
(31) Lee, C. Y.; Mccammon, J. A.; Rossky, P. J. *J. Chem. Phys.* **1984**, *80*, 4448.
(32) Tildesley, D. J.; Allen, M. P. *Computer Simulation of Liquids*; Clarendon Press: Oxford, 1987.
(33) Berendsen, H. J. C.; Postma, J. P. M.; Vangunsteren, W. F.; Dinola, A.; Haak, J. R. *J. Chem. Phys.* **1984**, *81*, 3684.
(34) Saff, E. B.; Kuijlaars, A. B. J. *Math. Intell.* **1997**, *19*, 5.
(35) Refson, K. *Comput. Phys. Commun.* **2000**, *126*, 310.
(36) Caillol, J. M.; Levesque, D.; Weis, J. J. *J. Chem. Phys.* **1986**, *85*, 6645.
(37) *CRC Handbook of Chemistry and Physics*, 85 ed.; CRC Press: 2004.
(38) Zasetsky, A. Y.; Khalizov, A. F.; Sloan, J. J. *J. Chem. Phys.* **2004**, *121*, 6941.
(39) Venables, D. S.; Schmuttenmaer, C. A. *J. Chem. Phys.* **2000**, *113*, 11222.
(40) Harris, F. J. *P. IEEE* **1978**, *66*, 51.
(41) Luzar, A.; Chandler, D. *J. Chem. Phys.* **1993**, *98*, 8160.
(42) Bergman, D. L.; Laaksonen, L.; Laaksonen, A. *J. Mol. Graph. Model.* **1997**, *15*, 301.
(43) Laaksonen, L. *J. Mol. Graphics* **1992**, *10*, 33.
(44) gOpenMol, version 3.0, http://www.csc.fi/gopenmol.